

**AD 696:440**

**TECHNICAL MEMORANDUM  
CAL NO. VJ-2330-G-53**

**A REPORT ON THE APPLICATION OF THE  
VISIOPLASTICITY METHOD TO SOFT-SOIL  
MOBILITY PROBLEMS**

**OFF-ROAD MOBILITY RESEARCH**

**Sponsored by:**

**Advanced Research Projects Agency**

**Project AGILE**

**Department of Defense**

**ARPA Order No. 841**

**Dated 7 May 1968**

**Under Contract DAHCO4 67 C 0005**

**U.S. Army Research Office - Durham**

**Durham, N.C. 27706**

**by:**

**P.M. MILLER**

**SEPTEMBER 1968**



**CORNELL AERONAUTICAL LABORATORY, INC.**

**OF CORNELL UNIVERSITY, BUFFALO, N. Y. 14221**

Reproduced by the  
**CLEARINGHOUSE**  
for Federal Scientific & Technical  
Information Springfield Va. 22151

51

**BEST  
AVAILABLE COPY**



CORNELL AERONAUTICAL LABORATORY, INC.  
BUFFALO, NEW YORK 14221

TECHNICAL MEMORANDUM  
CAL NO. VJ-2330-G-53

A REPORT ON THE APPLICATION OF THE  
VISIOPLASTICITY METHOD TO SOFT-SOIL  
MOBILITY PROBLEMS

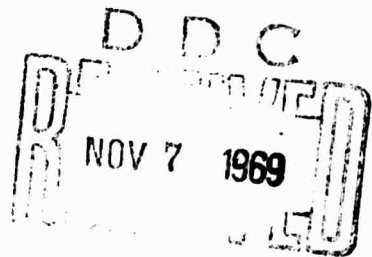
by  
P.M. Miller  
SEPTEMBER 1968

This document has been approved  
for public release and sale; its  
distribution is unlimited.

OFF-ROAD MOBILITY RESEARCH

Sponsored by:  
Advanced Research Projects Agency  
Project AGILE  
Department of Defense  
ARPA Order No. 841  
Dated 7 May 1966

Under Contract DAHCO4 67 C 0005  
U.S. Army Research Office - Durham  
Durham, N.C. 27706



## ABSTRACT

The viscoplasticity method of analysis, employed extensively in investigations related to metal processing problems, is applied to an analysis of a rigid wheel traversing a soft soil where flow is confined to two dimensions. Emphasis is placed on the way data taken from X-ray photographs are reduced in order to obtain the velocity, strain-rate and strain patterns for this flow condition. Consideration is given to modeling the dominant constitutive or material behavior and how this is incorporated along with the governing continuum field equations to provide calculations of the energy dissipation rate and the stresses acting on the wheel. Experimental data obtained by McGill University is used to illustrate the feasibility of this approach.

This method of analysis appears to be a very promising technique for investigating soft-soil mobility problems. The need for better experimental controls, particularly in soil preparation and simultaneous flow-field visualization, and possible future applications of the technique are indicated.

## FOREWORD

The research reported herein was performed by Cornell Aeronautical Laboratory, Inc. (CAL), and is a segment of the Soil Mechanics Task of the Off-Road Mobility Research (ORMR) program sponsored by OSD/ARPA for which CAL is the prime contractor and the U. S. Army Research Office - Durham is the contracting agency. The reported study is part of a broad research program designed to acquire off-road mobility knowledge; develop analysis, prediction and decision methodologies; and organize knowledge and methods to facilitate use by military planners, vehicle designers and field personnel concerned with off-road mobility. Under these broad objectives, soil mechanics research is directed at developing techniques for analyzing off-road mobility problems related to soft-soil conditions. The present study demonstrates the application of a technique used in metal processing analysis, called the viscoplasticity method, to a two-dimensional rigid wheel in soft clay. The study was performed during the period November 1967 - September 1968, under the guidance of Mr. George Bartlett, ORMR Program Manager. Mr. A. N. Tedesco was ARPA Technical Monitor.

Methods for data reduction and computer coding were developed by Messrs. John M. Grace and Seymour Samet, and Mrs. Miriam J. Watson. All experimental data used in this study was obtained under ORMR sub-contract by the McGill University Soil Mechanics Group under the direction of Prof. Raymond N. Yong. During the course of this study, Professor Yong has also provided many helpful ideas concerning the development of the analytical techniques.

## TABLE OF CONTENTS

	<u>Page</u>
ABSTRACT.....	ii
FOREWORD.....	iii
LIST OF ILLUSTRATIONS.....	vi
NOMENCLATURE.....	vii
1. INTRODUCTION.....	1
2. EXPERIMENTAL MEASUREMENTS AND DATA REDUCTION	4
2.1 Experimental Measurements.....	4
2.2 Calculation of the Velocity Field.....	5
2.3 Calculation of Strain-Rate Fields.....	6
2.4 Calculation of Equivalent Strain Field.....	8
3. MECHANICAL PROPERTIES OF THE SOIL MEDIUM....	9
3.1 Soil Behavior and Loading Conditions.....	9
3.2 Levy-Mises Plasticity Equations.....	10
3.3 Bingham, Viscoplastic Equations.....	12
4. CALCULATION OF LOAD VARIABLES.....	14
4.1 Determination of Energy Dissipation Rate.....	14
4.2 Calculation of Soil - Wheel Interface Stresses.....	15
5. FUTURE RESEARCH.....	19
5.1 Soil Preparation and Mechanical Properties.....	19
5.2 Types of Off-Road Loading Experiments.....	21
REFERENCES.....	28
APPENDIX I: COORDINATE TRANSFORMATIONS AND DATA- SMOOTHING TECHNIQUES.....	30
I-1. Coordinate Transformations.....	30
I-2. Data Smoothing of Flow Pattern.....	31
I-3. Velocity Interpolation Scheme.....	31

TABLE OF CONTENTS (Cont'd)

	<u>Page</u>
APPENDIX II: TENSOR NOTATION AND DEFINITIONS.....	34
APPENDIX III: CYLINDRICAL SOIL MECHANICS TEST.....	36
APPENDIX IV: CALCULATION OF STRESSES IN THE SOIL - WHEEL INTERFACE.....	38

## LIST OF ILLUSTRATIONS

<u>Figure</u>		<u>Page</u>
1	Soil Motion Pattern as Determined from Lead Markers (Three-Percent Slip)	23
2	Cutout Showing Checkerboard Pattern of Marker and Velocity Points	24
3	Equivalent Stress Vs. Equivalent Strain Relation Determined from Triaxial Test	25
4	Energy Dissipation Rate Shown as a Function of Slip	25
5	Stress Distribution Calculated for Rigid Wheel Having Three-Percent Slip	26
I-1	Schematic Representation Showing Experimental Facility	33
IV-1	Coordinate System Used for Stress Analysis	41

## NOMENCLATURE

$D$	drawbar pull force
$\dot{E}$	rate of external energy input
$\dot{E}_i$	rate of internal energy dissipation
$\dot{E}_s$	rate of surface energy dissipation
$e_{ij}$	strain deviator tensor
$\dot{e}_{ij}$	strain-rate deviator tensor
$\epsilon_{ij}$	strain tensor
$\dot{\epsilon}_{ij}$	strain-rate tensor
$\bar{\epsilon}$	equivalent strain
$\dot{\bar{\epsilon}}$	equivalent strain rate
$F$	yield function
$J_2$	second invariant of stress deviator tensor
$k$	yield stress in pure shear
$\dot{\lambda}$	plastic scalar proportionality function
$\mu$	kinematic viscosity coefficient
$p$	hydrostatic pressure
$R$	wheel radius
$r, \theta$	polar coordinate variables
$s_{ij}$	stress deviator tensor
$\sigma_{ij}$	stress tensor
$T$	wheel torque
$t$	time variable
$u$	$x$ component of velocity vector

$v$   $y$ -component of velocity vector  
 $V$  wheel linear velocity  
 $W$  wheel load  
 $x, y$  Cartesian coordinate variables

## 1. INTRODUCTION

The role of soft soil in the generation of tractive forces acting on off-road vehicles has been under investigation for a number of years. [1, 2] The problem is generally recognized as one having mixed boundary conditions with large inelastic sinkage where significant energy is dissipated within the soil medium. However, surprisingly little effort has been directed toward making measurements within the soil, and most research effort is restricted to measuring only external parameters such as drawbar pull, torque, normal load and slip. Furthermore, the soil properties are usually described as being either cohesive or frictional, with little consideration given to the soil state.

Most attempts to analyze these problems have avoided the mathematical difficulties by making some far-reaching assumptions concerning the soil behavior under off-road loading conditions. Although these assumptions may make the problem mathematically tractable, they inevitably lead to engineering models which do not satisfy basic continuum mechanics field equations. In this sense, these engineering models do not explain the physical mechanism responsible for the generation of tractive forces on the vehicle.

If these problems are approached in a purely analytical manner, it soon becomes apparent that suitable analytical techniques are not likely to be developed in a reasonable time period. As a result, Cornell Aeronautical Laboratory, under the Soil Mechanics Task of the Off-Road Mobility (ORMR) Program, proposed to investigate these problems on a somewhat fundamental level with a limited effort, guided by two prime considerations: (a) the solutions must be based on continuum mechanics principles with recognition given to the particulate nature of the material, and (b) the techniques which are developed must be generally applicable to all types of off-road loading conditions. [3]

Within this framework, it was decided that the probability of success would be much higher if combined analytical, empirical techniques were employed. The results obtained during the past fifteen years with

the visioelasticity method in metal processing analysis were particularly impressive. [4, 5, 6, 7] Furthermore, it appeared that this technique, along with suitable modification, could be employed in investigations of typical off-road loading situations. [8]

The visioelasticity method assumes that the velocity field can be determined experimentally, and that the stresses can be obtained analytically from these measurements. That is, the strains and strain rates are calculated directly from the velocity field while the stress distribution results from an analytical solution of the equilibrium (or motion) equations and the constitutive equation relating the stress and strain for the material.

This technique has been extensively applied in metal processing analysis where the velocity fields are determined by photographing grids attached to the surface of the workpiece. Photographs are usually taken after successive incremental displacements. The material is assumed to behave as a Levy-Mises, rigid, perfectly plastic solid.

The application of this technique to soil mechanics problems requires further experimental effort in three areas: (a) measurement of the displacements, (b) preparation of the soil medium, and (c) the determination of the soil mechanical properties. McGill University has successfully developed and employed the pulsed X-ray technique to measure soil displacements. [9, 10, 11] In addition, some success using a technique similar to the visioelasticity method has been reported at Cambridge University where foundation-type problems were investigated. [12, 13] Soil preparation and the determination of the mechanical properties requires a continuing effort and has been under study at Cornell University. [14, 15]

The present soil mechanics work has been restricted to the behavior of nearly saturated clays at high water contents. Because such materials generally exhibit little internal friction, a plasticity theory would be expected to be most promising with this type of soil. Fortunately, such soils are of prime interest in soft-soil mobility problems. [14]

The purpose of the present study was to determine if the visio-  
plasticity method is a reasonable way to analyze the typical off-road  
loading situation. A rigid wheel was selected for the study because  
steady-state behavior could be assumed and McGill University was  
prepared to make the measurements on such a wheel. It was initially  
recognized that full utilization of this technique would eventually require  
the instantaneous visualization of the entire flow field and a better speci-  
fication of the soil mechanical properties. However, it was felt that,  
rather than go to the expense of constructing elaborate facilities, it might  
be wise to use existing facilities and techniques to test the validity of this  
method. In this sense, the results of this initial investigation must be  
viewed in a qualitative manner.

If it is possible to use this technique to analyze these problems,  
then the solutions should be exact in the engineering sense. Such solutions  
can serve as the basis for verification and formulation of engineering models.  
The present report concerns itself with an illustration of how the visio-  
plasticity method can be applied to a specialized situation. At a later date, the results  
obtained from this study will be compared with those of other specific engi-  
neering models.

## 2. EXPERIMENTAL MEASUREMENTS AND DATA REDUCTION

### 2.1 Experimental Measurements

All experimental data used in this study were developed by McGill University under ORMR subcontract and a detailed discussion of their experimental facilities is available in Reference 11. To set the stage for the subsequent analysis and discussion, only a brief description of the soil preparation process and the type of experiment are presented.

To develop the soil test bed with lead markers in the wheel mid-plane, a dry kaolinite is placed in alternating layers with a prescribed amount of water (approximately 50 percent by weight) and allowed to rest until the water migration is equilibrated. The soil test bed is then built up from this material in layers through a process of remolding small quantities and tamping them into position. It should be noted that the soil is built up so that the plane of the markers is horizontal. The lead markers are embedded when the layering is one-half the required depth. When the test bed preparation is completed, the bed is rotated so that the marker plane is vertical and in the midplane of the wheel. Walls are maintained along the sides of the soil so as to prevent any side flow.

A carriage traveling at a constant velocity carries a rigid, 13.5-inch-diameter wheel having a width of 3.75 inches, equal to that of the soil test bed. In addition to the linear velocity, an angular velocity is imposed on the wheel. Transducers located on both the carriage yolk and the wheel axle shaft measure the drawbar pull and torque acting on the wheel. Sinkage is recorded by measuring the relative distance between the wheel center and side rails.

Before, during, and after a test run, X-ray photographs are taken for a 6- by 7-inch area (in the marker plane). Three X-rays are shot during the test with each shot separated by the time required for the wheel to traverse 6 inches. Thus, in a coordinate system moving with the wheel, these three X-ray shots map out the soil displacements

over an area approximately 18 by 7 inches. In this system, the X-ray measurements are equivalent to the displacement time history for the soil motions.

It is readily seen that the marker measurements are taken in a system fixed to the X-ray unit or fixed in physical space. In this system, the soil motion must be viewed as unsteady. If, however, the coordinates of the markers are viewed relative to a coordinate system attached to the wheel, then it seems reasonable to assume a steady-state motion for constant wheel velocities. Since steady-state motion has been assumed in the analysis, the measurements are transformed to coordinates attached to the wheel axle. This simple transformation, along with data-smoothing techniques, is shown in Appendix I.

## 2.2 Calculation of the Velocity Field

The marker positions relative to the wheel are shown in Figure 1. In this analysis, we assume that the markers shown in any row are deformed from an initial, horizontal, straight line of markers. Consistent with the steady-state assumption, any row of markers can be taken as either a streamline or a path line for a material particle. Movement along a row from right to left is equivalent to following the motion or time history of a particle. Since the time increments between markers may be determined from the distance between these markers in the initial or undeformed configuration and the wheel axle velocity, the relative time history for any marker is known.

The results shown in Figure 1 represent some smoothing and the precise procedure is given in Appendix I. Nevertheless, these coordinate points are used to determine the velocity field. As shown, a triangular array of markers was employed in the marker plane. Shown in Figure 2 is a cutout indicating both marker points and velocity points. If we consider the point  $(i, j)$  and its neighboring points, then the  $x$  and  $y$  components of the velocity vector,  $u$  and  $v$ , respectively, are defined

at the point  $(i+1, j)$  according to

$$\begin{aligned} u_{i+1, j} &= \frac{x_{i+2, j} - x_{i, j}}{\Delta t_i} \\ v_{i+1, j} &= \frac{y_{i+2, j} - y_{i, j}}{\Delta t_i} \end{aligned} \quad (2.1)$$

The time increment,  $\Delta t_i$ , is determined from the initial coordinate distances; i. e.,

$$\Delta t_i = \frac{x_{i+2, j}^i - x_{i, j}^i}{V} \quad (2.2)$$

where the superscript  $i$  indicates initial positions (from first X-ray shot) and  $V$  is the wheel axle velocity.

In this manner, the data are tabulated in a checkerboard pattern where particle positions, defined at marker points, alternate with velocity component points defined at midpoints between successive markers in the same row. The velocities are now used to determine strain rates and strains at the marker points.

### 2.3 Calculation of Strain-Rate Fields

Since uniform strain conditions are assumed throughout the soil thickness and no side flow is permitted, the only nonzero components of the strain-rate tensor are  $\dot{\epsilon}_x$ ,  $\dot{\epsilon}_y$ , and  $\dot{\epsilon}_{xy}$ . In terms of the velocity components,  $u$  and  $v$ , these components are

$$\dot{\epsilon}_x = \frac{\partial u}{\partial x}, \quad \dot{\epsilon}_y = \frac{\partial v}{\partial y}, \quad \dot{\epsilon}_{xy} = \frac{1}{2} \left( \frac{\partial u}{\partial y} + \frac{\partial v}{\partial x} \right). \quad (2.3)$$

Thus, if the first derivatives of the velocity components are known at the marker points, then the strain-rate tensor is also known.

The triangular array was selected primarily because of these derivatives. For example, with a central difference approximation, the partial derivatives of  $u$  with respect to  $x$  and  $y$  at the point  $(i, j)$

(see Figure 2) are taken as

$$\left(\frac{\partial u}{\partial x}\right)_{i,j} \approx \frac{u_{i+1,j} - u_{i-1,j}}{x_{i+1,j} - x_{i-1,j}}$$

$$\left(\frac{\partial u}{\partial y}\right)_{i,j} \approx \frac{u_{i,j+1} - u_{i,j-1}}{y_{i,j+1} - y_{i,j-1}} \quad (2.4)$$

Similar approximations could be made for the derivatives of  $v$ .

Since finite strains are evident, corrections due to the geometry changes must be incorporated into the above approximations. This was done by fitting surfaces to the  $u$  and  $v$  velocity components. Some smoothing is also employed in this process and again the details are given in Appendix I. Since the distance between marker points is about one inch, the derivatives in Equation (2.4) are actually determined according to

$$\left(\frac{\partial u}{\partial x}\right)_{i,j} = u(x_{i,j} + 0.5, y_{i,j}) - u(x_{i,j} - 0.5, y_{i,j})$$

$$\left(\frac{\partial u}{\partial y}\right)_{i,j} = u(x_{i,j}, y_{i,j} + 0.5) - u(x_{i,j}, y_{i,j} - 0.5) \quad (2.5)$$

where the  $u$  values are taken from the surface-fit function about the point  $(i,j)$  for the  $u$  velocity component. It is clear that, with this scheme, the velocity values are interpolated near the velocity points.\*

For the analysis, an equivalent strain rate (see Section 3) is required. In the plane strain problem, the equivalent strain rate,  $\dot{\bar{\epsilon}}$ , is given by

$$\dot{\bar{\epsilon}} = \frac{2}{3} \left[ \dot{\epsilon}_x^2 - \dot{\epsilon}_x \dot{\epsilon}_y + \dot{\epsilon}_y^2 + 3\dot{\epsilon}_{xy}^2 \right]^{\frac{1}{2}} \quad (2.6)$$

---

\*It should be noted that, because polynomials up to second order are used in the surface fit, this scheme is equivalent to differentiation of the surface and evaluation at the point  $(i,j)$ .

This quantity is essentially the second invariant of the strain-rate tensor (within a constant multiple) and is, consequently, a scalar function independent of coordinate transformations.

#### 2.4 Calculation of Equivalent Strain Field

In order to incorporate the stress-strain properties into the analysis, it is necessary to determine an equivalent strain parameter. By definition, the equivalent strain,  $\bar{\epsilon}$ , is

$$= \int_{t_0}^t \dot{\bar{\epsilon}} dt \quad (2.7)$$

where the integration, with respect to time, is taken along the particle path. This integration is readily performed along the path lines or streamlines as determined from Figure 1.

### 3. MECHANICAL PROPERTIES OF THE SOIL MEDIUM

#### 3.1 Soil Behavior and Loading Conditions

In a system of continuum mechanics field equations, the constitutive equation is a tensor equation which describes the mechanical properties of the medium. Various physical behavior, such as elastic, plastic or viscous properties, can be modeled by appropriate terms in the constitutive equation. However, since precise accounting of all these phenomena leads to an extremely complicated system of field equations, a realistic application of continuum mechanics to most problems requires that only the more dominant aspects of the material properties be modeled.

The dominant mechanical properties exhibited by materials result from the material state and the loading conditions. Specifically, fine grain soils are a problem to military vehicle mobility when they are at high water content and near full saturation.<sup>[14]</sup> Furthermore, the loading on the soil occurs over a short time period (measured in seconds). The maximum or limiting stress conditions are reached causing considerable soil flow and, upon unloading, there is little elastic strain recovery. As a result, it seems appropriate to initially restrict primary attention to a two-phase water and fine-grain particle material.

In considering a two-phase medium such as a saturated clay, the important factor to consider is the relative load velocities of the water and solid phases under the loading conditions. The small amount of drainage which occurs under rapid loadings indicates that this relative velocity is small. Consequently, for off-road loading rates, it would seem appropriate to consider the soil as a single, continuous, incompressible medium and employ total rather than effective stresses.

Since the loading condition subjects the soil to large strains and limiting stress conditions, our initial approach relies on a purely plastic constitutive equation. Because of the high water content, the limiting stress may tend to depend upon the rate of loading. Such materials exhibiting viscous effects will require a more refined theory relying upon viscoplastic constitutive theory.

In the following, simplified rigid-plastic and rigid-viscoplastic constitutive equations are discussed. These include Levy-Mises plasticity and the Bingham viscoplastic relations. Although each of these relations has been applied primarily in other areas, the governing conditions for the fine grain soils indicate that these constitutive theories should, with suitable modification, provide reasonable first-order approximations for modeling the material behavior. A detailed derivation of these equations can be found in other sources (e. g., see Prager, Reference 16).

### 3.2 Levy-Mises Plasticity Equations

The Levy-Mises plasticity equations assume that (a) the flow is incompressible, (b) there is no recoverable strain upon unloading, and (c) the directions of the principal axes of the stress deviator tensor and those of the strain-rate deviator tensor coincide. The tensor equation becomes

$$\dot{\epsilon}_{i,j} = \begin{cases} 0 & \text{if } F < k^2 \\ \lambda S_{ij} & \text{if } F = k^2 \end{cases} \quad (3.1)$$

where  $\dot{\epsilon}_{i,j}$  is the strain-rate deviator tensor,  $S_{ij}$  the stress deviator tensor,  $\lambda$  a scalar proportionality function,  $F$  the yield function, and  $k$  the yield stress in pure shear.\*

These equations must be augmented by a suitable yield condition. For the Mises yield condition, the function  $F$  is equal to the second invariant,  $J_2$ , of the stress deviator tensor. Thus,

$$J_2 = k^2 \quad (3.2)$$

is the generalized representation of the Mises yield condition. It should be noted that the yield condition could be replaced by some other constraint such as the Mohr-Coulomb or Tresca yield conditions.

---

\* See Appendix II for brief review of the tensor notation and definitions.

For a rigid, perfectly plastic theory,  $k$  in Equation (3.2) is constant but for a work-hardening material,  $k$  depends upon the strain history. There exists considerable evidence that, with saturated, fine grain clays, some yielding occurs with initial loading. In addition, with continued loading, the yield stress increases in a manner similar to a work-hardening material. Consequently, in the representation of this soil behavior, it is further assumed that a yield surface is formed upon initial loading and that this surface expands with continued loading.

As a result of this latter assumption and that of material incompressibility (i. e., the strain-rate tensor is equal to the strain-rate deviator tensor), Equation (3.1) becomes

$$\dot{\epsilon}_{i,j} = \dot{\lambda} S_{i,j} \quad (3.3)$$

with

$$F = J_2 = k^2 \quad (3.4)$$

where now  $k$  is taken as a function of the strain and  $\dot{\epsilon}_{i,j}$  is the strain-rate tensor. The scalar function,  $\dot{\lambda}$ , in Equation (3.3) must be determined by experimentation. The usual procedure is to use the tensor scalar product to square both sides of Equation (3.3). Thus,

$$\dot{\lambda} = \frac{\sqrt{\dot{\epsilon}_{i,j} \dot{\epsilon}_{i,j}}}{\sqrt{S_{i,j} S_{i,j}}} \quad (3.5)$$

where repeated subscripts indicate summation.

Following Hill [17], we may define an equivalent strain rate,  $\dot{\bar{\epsilon}}$ , and an equivalent stress,  $\bar{\sigma}$ , as

$$\begin{aligned} \dot{\bar{\epsilon}} &= \sqrt{\frac{2}{3} \dot{\epsilon}_{i,j} \dot{\epsilon}_{i,j}} \\ \bar{\sigma} &= \sqrt{\frac{2}{3} S_{i,j} S_{i,j}} \end{aligned} \quad (3.6)$$

\*With this definition of  $\bar{\sigma}$ , the relationship between  $\bar{\sigma}$  and  $J_2$  is  $\bar{\sigma} = \sqrt{3J_2}$  and, according to Equation (3.4),  $\bar{\sigma} = \sqrt{3} k$ .

As a result of these definitions, Equation (3.3) becomes

$$\dot{\epsilon}_{ij} = \frac{3}{2} \frac{\dot{\bar{\epsilon}}}{\bar{\sigma}} s_{ij}. \quad (3.7)$$

It is necessary to determine a test which will provide an equivalent stress versus equivalent strain curve. For metals, this relationship is usually determined by a uniaxial compression test. With soft soils, however, this kind of test is difficult to perform and, in Appendix III, we show how the results of a typical soil mechanics cylindrical (triaxial) test can be interpreted as an equivalent stress versus equivalent strain curve.

A typical equivalent stress versus equivalent strain curve for the remolded kaolinite used in the soil test bed is shown in Figure 3. Stress-strain results were obtained by McGill University for cylindrical samples under undrained conditions. A number of tests were conducted and some variation was experienced. The curve shown was used in subsequent analysis and represents a medium for the tests. Since the analysis requires deformation rates, the "natural" or logarithmic strain has been used.

For the analysis, the hyperbolic strain relation, developed for metals by Cox [18] and used extensively by Kondner [19] has been used to fit the equivalent stress versus equivalent strain curve. The curve-fit relation for the results shown in Figure 3 is

$$\bar{\sigma} = \frac{\bar{\epsilon}}{0.048 + 0.2785 \bar{\epsilon}}. \quad (3.8)$$

In the computer calculations, this equation was used to relate equivalent stress to equivalent strain.

### 3.3 Bingham, Viscoplastic Equations

The constitutive equation for the incompressible Bingham solid is

$$2\mu \dot{\epsilon}_{ij} = \begin{cases} 0 & \text{if } \sqrt{J_2} \leq k \\ \frac{\sqrt{J_2} - k}{\sqrt{J_2}} s_{ij} & \text{if } \sqrt{J_2} > k \end{cases} \quad (3.9)$$

where  $\mu$  is a kinematic viscosity coefficient,  $J_2$  the second invariant of the stress deviator tensor,  $k$  the static shear yield stress,  $\dot{\epsilon}_{ij}$  the strain-rate tensor and  $S_{ij}$  the stress deviator tensor. Again, if yielding is assumed to occur on initial loading, then Equation (3.9) becomes

$$\dot{\epsilon}_{ij} = \frac{\frac{1}{2} \dot{\bar{\epsilon}}}{\sigma + 3\mu \dot{\bar{\epsilon}}} S_{ij} \quad (3.10)$$

when equivalent stress and strain rate are employed.

It should be noted that, for no viscous effects (i. e., for  $\mu=0$ ), Equation (3.10) reduces to the Levy-Mises plasticity relation, Equation (3.6). Consequently, the Bingham relation, as given here, may be taken as a first-order extension into the dynamic or viscous range of the static plasticity theory.

There are a number of other possible material representations for viscoplastic solids. A clear discussion of the constitutive theory for these materials is given by Perzyna.<sup>[20]</sup> The selection of a suitable material representation will require extensive testing of the material at various loading rates. Nevertheless, in view of favorable results reported concerning mud-drilling investigations,<sup>[21]</sup> the immediate extension of the plastic results to a viscoplastic theory should undoubtedly employ the generalization of the linear Bingham solid.

In this report, no calculations are performed using a viscoplastic theory. It appears, however, that the viscoplasticity method could be readily extended to include this kind of dynamic behavior.

#### 4. CALCULATION OF LOAD VARIABLES

Once the kinematic variables are determined experimentally and the soil mechanical properties known, the viscoplasticity theory may be used to determine the loads (forces and stresses) acting on the wheel. In the following, consideration is given to both the determination of the energy dissipation rate within the soil medium and to the stresses acting in the soil - wheel interface.

##### 4.1 Determination of Energy Dissipation Rate

According to the limit analysis theorems of Drucker, et. al. [22] the following inequality holds for any kinematically admissible velocity field

$$\dot{E} \leq \int_V \bar{\sigma} \dot{\bar{E}} dV + \int_S k \Delta V ds \quad (4.1)$$

where  $\dot{E}$  is the rate of external energy input,  $\bar{\sigma}$  the equivalent stress,  $\dot{\bar{E}}$  the equivalent strain rate for the elemental volume  $dV$ ,  $k$  the shear strength, and  $\Delta V$  the velocity discontinuity along the surface  $S$ .<sup>\*</sup> With the viscoplasticity method, the velocity field is measured and is, consequently, the actual velocity field. As a result, the equal sign may be taken in Equation (4.1). Furthermore, with the rigid-wheel, soft-soil problems, the only observable velocity jump occurs along the soil - wheel interface.

For the rigid wheel case, let

$$\dot{E} = \dot{E}_i + \dot{E}_s \quad (4.2)$$

where the rate of internal energy dissipation,  $\dot{E}_i$ , is given by

$$\dot{E}_i = \int_V \bar{\sigma} \dot{\bar{E}} dV \quad (4.3)$$

and the surface dissipation,  $\dot{E}_s$ , by

$$\dot{E}_s = \int_S k \Delta V ds \quad (4.4)$$

<sup>\*</sup>This would require some modification if a viscoplastic theory were employed.

with  $t$  the soil shear strength and  $\Delta V$  the velocity jump between the wheel and soil surfaces. Both of these energy dissipation components are readily determined once the stress-strain and kinematic properties are known.

The energy dissipation calculations for three tests are shown in Figure 4 and Table I. Also shown are the energy input, as determined from the measured external loads, and velocities. Since the linear velocities do not vary over a large range (see Table I), the energy dissipation is shown as a function of slip. However, for large variations in the linear velocities, some other time-dependent variable would probably be more appropriate.

Significantly, the results indicate that energy is dissipated in two ways because of the stress and strain-rate fields in the soil medium and as a result of a velocity discontinuity between the soil and the wheel surface. In addition, the energy dissipated in the soil medium appears to show some variation with slip (at almost constant linear velocity) while that in the interface is very dependent upon the slip. This latter phenomenon requires further investigation.

For the wheel having a constant velocity, the energy dissipation may be interpreted in terms of an equivalent drag force acting upon the wheel. For example, if we divide by a standard length per unit time (i. e., the wheel linear velocity), then

$$F_D = \frac{\dot{E}}{V} \quad (4.5)$$

may be taken as an equivalent drag force acting upon the wheel.

It is desirable to have the actual stresses acting in the soil - wheel interface. In the following, we show how these stresses may be calculated for the rigid wheel. In the analysis, we permit velocity discontinuities across viscous layers of high energy dissipation but no stress discontinuities are permitted.

#### 4.2 Calculation of Soil - Wheel Interface Stresses

Within the soil - wheel interface, the stresses  $\sigma_r$ ,  $\sigma_\theta$  and  $\tau_{r\theta}$  are determined by the following equations (see Appendix IV for the derivation)

$$\begin{aligned}
\sigma_r &= \frac{2}{3} \left\{ \left[ \frac{\bar{\sigma}}{\bar{\epsilon}} (\dot{\epsilon}_r - \dot{\epsilon}_\theta) \right]_{\theta_0}^{\theta} - R \int_{\theta_0}^{\theta} \left[ \frac{1}{2} \frac{\partial}{\partial r} \left( \frac{\bar{\sigma}}{\bar{\epsilon}} \dot{\gamma}_{r\theta} \right) + \frac{1}{R} \frac{\bar{\sigma}}{\bar{\epsilon}} \dot{\gamma}_{r\theta} \right] d\theta' \right\}_{r=R} \\
\sigma_\theta &= \sigma_r - \left[ \frac{2}{3} \frac{\bar{\sigma}}{\bar{\epsilon}} (\dot{\epsilon}_r - \dot{\epsilon}_\theta) \right]_{r=R} \\
\tau_{r\theta} &= \left[ \frac{1}{3} \frac{\bar{\sigma}}{\bar{\epsilon}} \dot{\gamma}_{r\theta} \right]_{r=R}
\end{aligned} \tag{4.6}$$

where, theoretically,  $\dot{\epsilon}_r$ ,  $\dot{\epsilon}_\theta$ ,  $\dot{\gamma}_{r\theta}$  and  $\bar{\epsilon}$  are strain rates determined from the velocity fields, while  $\bar{\sigma}$  is the equivalent stress taken from the stress-strain curve, Equation (3.8).

From the kinematic measurements,  $\dot{\epsilon}_x$ ,  $\dot{\epsilon}_y$ ,  $\dot{\gamma}_{xy}$ ,  $\bar{\epsilon}$  and  $\bar{\sigma}$  are known at discrete points throughout the soil medium. For the polar coordinate system used in the derivation of Equations (4.6), the Cartesian strain-rate components are readily transformed at each discrete point to the polar form by

$$\begin{bmatrix} \dot{\epsilon}_r - \dot{\epsilon}_\theta \\ \dot{\gamma}_{r\theta} \end{bmatrix} = \begin{bmatrix} \cos 2\theta & \sin 2\theta \\ -\sin 2\theta & \cos 2\theta \end{bmatrix} \begin{bmatrix} \dot{\epsilon}_x - \dot{\epsilon}_y \\ \dot{\gamma}_{xy} \end{bmatrix} \tag{4.7}$$

while the quantities  $\bar{\epsilon}$  and  $\bar{\sigma}$  are invariants and remain unchanged with the change in coordinates.

The same general surface fitting routine which was used in the determination of the kinematic variables is again employed to interpolate the desired values on the soil - wheel interface. For this fit, triangular arrays of fifteen points are used to successively interpolate the desired values at about one-inch intervals in the soil - wheel interface.

The stress results for the test having the lowest slip in Table I are shown in Figure 5. The routine is currently being run for other tests, and it is anticipated that they will be reported in a separate report. As can be observed from Equations (4.6), we would expect the results for the shear stress,  $\tau_{r\theta}$ , to probably be somewhat better since integration is not involved. The determination of the radial stress,  $\sigma_r$ , is more

complicated since two angles,  $\theta_0$  and  $\theta_m$ , must be determined in order to perform the integration. It is difficult to estimate these angles using the X-ray measurements. Furthermore, the results for  $\sigma_r$  are dependent upon the value taken for  $\theta_0$ . These kinematic quantities in the soil - wheel interface might be better determined by augmenting the X-ray measurements with photographs of surface grids through glass walls.

Some comments concerning the calculated stress distribution are in order. The radial stress appears to reach a maximum value near the point where the soil enters the interface. This is in contradiction to the plate-sinkage models, where the maximum radial stress is obtained at the point of maximum sinkage. The shear stress takes on its maximum value near the bottom of the wheel. As the soil enters the interface region, this maximum is reached gradually but, once reached, it tends to remain constant.

The results might be compared to those of Onafeko and Reece<sup>[23]</sup> where stress measurements were made on a rather large wheel (49-inch diameter). These results tend to exhibit some of the trends measured; e. g., maximum radial stress is built up quickly in the contact region. It should be observed, however, that a comparison is not necessarily appropriate since the Onafeko-Reece results are for a much larger scale and, also, their problem has three-dimensional flow contrasted to the two-dimensional constants considered here.

To compare the stresses with the measured loads, the following equations were used:

$$\begin{aligned}
 T &= (6.75)^2 (3.75) \int_{\theta_0}^{\theta_m} \tau_{r\theta} d\theta \\
 W &= (6.75)(3.75) \left[ \int_{\theta_0}^{\theta_m} (\sigma_r \sin \theta - \tau_{r\theta} \cos \theta) d\theta \right] \\
 D &= (6.75)(3.75) \left[ \int_{\theta_0}^{\theta_m} (\tau_{r\theta} \sin \theta - \sigma_r \cos \theta) d\theta \right]
 \end{aligned}
 \tag{4.8}$$

where  $T$  is torque,  $W$  is the normal load, and  $D$  is the drawbar pull. The calculated values were 106 inch-pounds, 50 pounds and zero (actually 0.25 pound), respectively, for the torque, load and drawbar pull. These correspond to measured values of 113 inch-pounds, 74 pounds, and a negative 3 pounds, respectively.

It is interesting that all of the calculated values are somewhat lower than those measured. In addition, the energy dissipation for this test was lower than that determined from the measurements. This possibly means that the stress-strain relation should be different than that used in the analysis. It would seem that this supports the assertion that better determination of the soil properties are needed.

## 5. FUTURE RESEARCH

The present results indicate that the visioelasticity method can be used to determine either the energy dissipation rate or the stresses within the soil medium. However, some improvement in both the soil preparation process and the measurement technique is necessary. These problems have been considered and, based upon the results of the Cornell University study,<sup>[15]</sup> various ways of preparing the soil medium appear feasible. The problem of measurement (namely, the instantaneous visualization of the flow field) may be obtained with commercially available pulse X-ray equipment, supplemented by surface grid photographs.

The visioelasticity method should be extended to other, more important loading conditions. Such extensions will require considerable effort in the development of analytical methods. This will undoubtedly require the application of numerical techniques to solve the governing equations.

### 5.1 Soil Preparation and Mechanical Properties

At present, the soil behavior in mobility research is assumed to be essentially the same as in foundation engineering problems. Because the limiting shear stresses exhibited by soils used for foundations are usually much higher than those exhibited by soft soil common to vehicle impedance, the application of traditional soil mechanics requires considerable extrapolation. Recent results obtained at Cornell University<sup>[15]</sup> indicate that the low strength behavior of highly saturated clays is considerably different than anticipated by traditional theory. These results indicate that, when kaolinite is consolidated to a low stress, it exhibits reasonable total stress-strain characteristics.

When considering the behavior of soft soils, attention must necessarily be focused on fine grain soils at high water content. These soils tend to be progressively weakened by repetitive loading. Such field behavior evidently results from considerable soil flow or shear distortion. On the other hand, when soils are normally prepared in soil bins, the preparation process includes combinations of soil remolding, tillage, etc.

When prepared in this manner, repeated loading will tend to compress the material resulting in a higher shear strength. It is imperative that soils be prepared in a carefully controlled manner so that they exhibit low strength characteristics and virtually incompressible flow.

It is recommended that some effort be directed toward preparing test beds from a slurry using an anisotropic overconsolidation process and, furthermore, that the mechanical properties be expressed in terms of total stresses rather than effective stresses.\* Although considerable effort would be required to prepare this kind of soil bed, the mechanical properties would be reasonably well defined using traditional soil mechanics equipment.

Some limited success might be obtained through the use of artificial soils where the fluid phase is replaced by an oil or some other medium. Such materials are more stable with time and might be more easily reproduced than clay - water systems. This type of material, however, should be expected to provide results over only a very limited range of soil behavior. Even though artificial soils might be developed so as to simulate the required stress-strain properties, it is doubtful that they could simulate the strength changes with repeated loadings.

More important, clays tend to take on water by swelling. This builds up pressures in the soil which causes the soil to be left in a state of overconsolidation upon drying. Such loading histories are perhaps most responsible for the state of fine grain clays when found under natural field conditions. It is highly unlikely that artificial soils could ever simulate this more fundamental behavior. Thus, it is reasonable to judiciously use some type of artificial soil in laboratory simulations but the broader aspects of the problem will require experimentation with clay - water systems.

---

\* Note, effective stresses are required to determine the degree of consolidation but the total stress concept should suffice during the vehicle loading simulation.

Some additional experimentation is required to determine the stress-strain properties for the model study materials. These tests, employing total stresses, should be performed with loading rates comparable to those observed in the vehicle loading simulation. In the rigid wheel tests, they were nominally about 0.25-inch/inch/second. Conventional undrained triaxial (cylindrical) tests performed near this rate in both the confined and unconfined conditions should be satisfactory. If the soil is found to be rate dependent, then some consideration must be given to a viscoplastic representation of the material.

## 5.2 Types of Off-Road Loading Experiments

Current methods of visualizing the soil flow pattern must be improved. The present method employs a 300-kv X-ray system which permits instantaneous visualization of an approximately 6- by 7-inch area. Recent studies at CAL indicate that this would be greatly enhanced with a newer 600-kv system. This system would permit the visualization of a circular area approximated by 30 inches in diameter.

It is recommended that this system be augmented by taking photographs of grids placed on the soil adjacent to a transparent, lubricated wall. The McGill University group has observed with simultaneous X-ray and photographic measurements that the wall effects may be important. [24] Nevertheless, the problem, particularly in the soil - vehicle interface, requires some high speed measurements which probably can only be obtained with photographic techniques.

The viscoplasticity method should be extended to other more important problems. We cite here two categories: (a) so-called running-gear elements, and (b) soil measuring instruments. Wheels, tracks, grousers, etc. are included in the former while indentors and soil-surface measuring devices make up the latter. If the kinematics of each problem can be adequately determined and the soil properties specified, then the viscoplasticity method could serve as a powerful tool for investigating the behavior within the soil and relating the mechanical properties to the external loads.

Although, in principle, the method could be utilized with three-dimensional problems, present investigations should be continued primarily with two-dimensional experiments. These should include a flexible wheel and a wheel - belt arrangement simulating a track. Such investigations would require additional analytical effort in order to determine the stresses. For example, in the rigid-wheel analysis, the stress solution is simplified since it is readily established that the radial stress component in the soil - wheel interface depends only upon the angular coordinate. This simplification would not be possible in an investigation of a flexible wheel where a numerical scheme would probably be required.

Present measuring instruments essentially attempt to relate measured forces, torques, etc. to limiting shear stresses. Because the boundary value problems have not been solved, these devices correlate the soil mechanical properties with measured loads in a purely empirical manner. A more precise investigation should shed some light on the kind of correlation and the number of tests required to draw the necessary conclusions regarding the soil state.

Finally, it should be observed that, even though the prime interest is currently with saturated, high-water content clays, eventually, some consideration will have to be given to other soils. Such investigations will again be most dependent upon the way the soil is modeled in the constitutive equation.

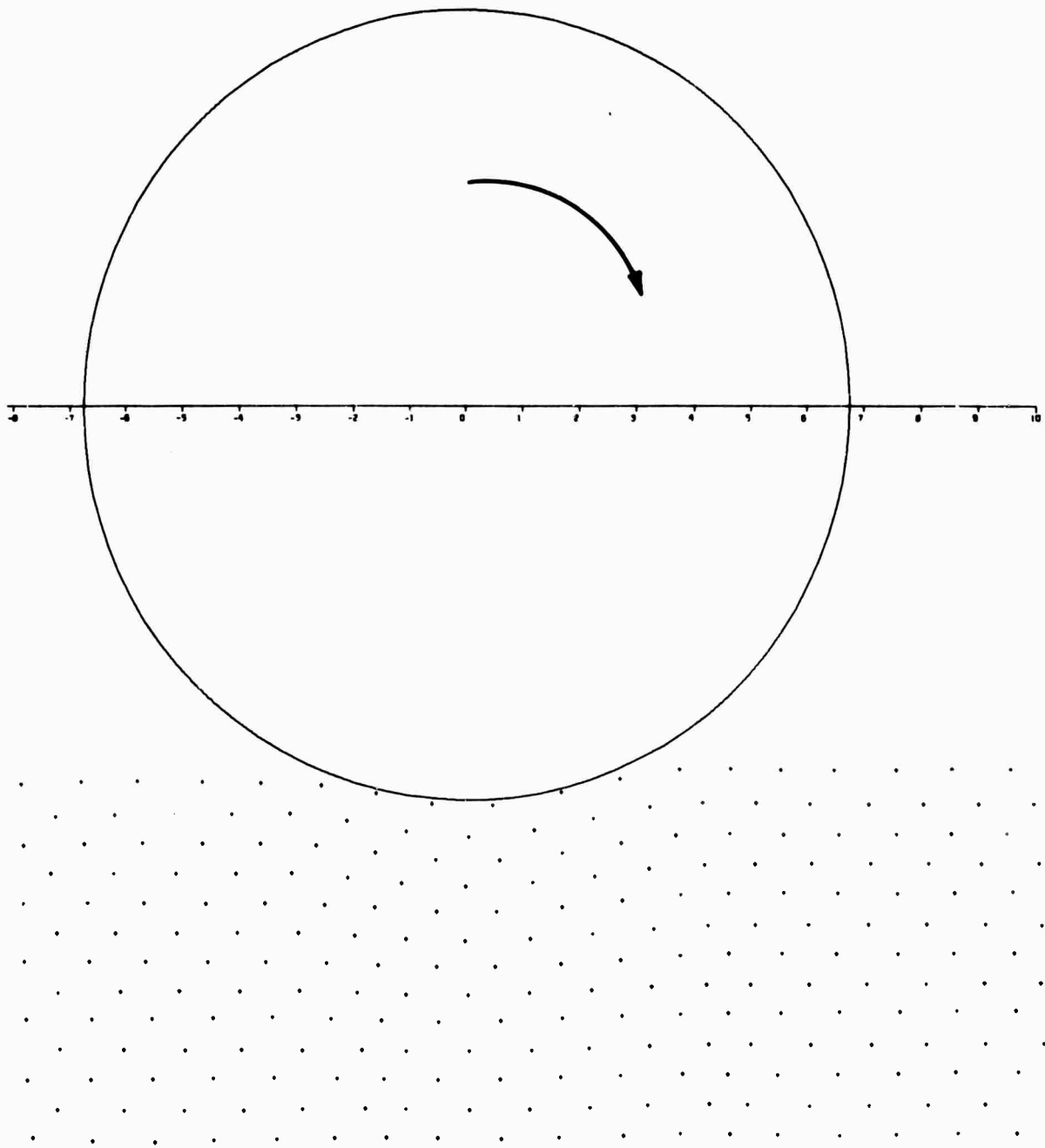
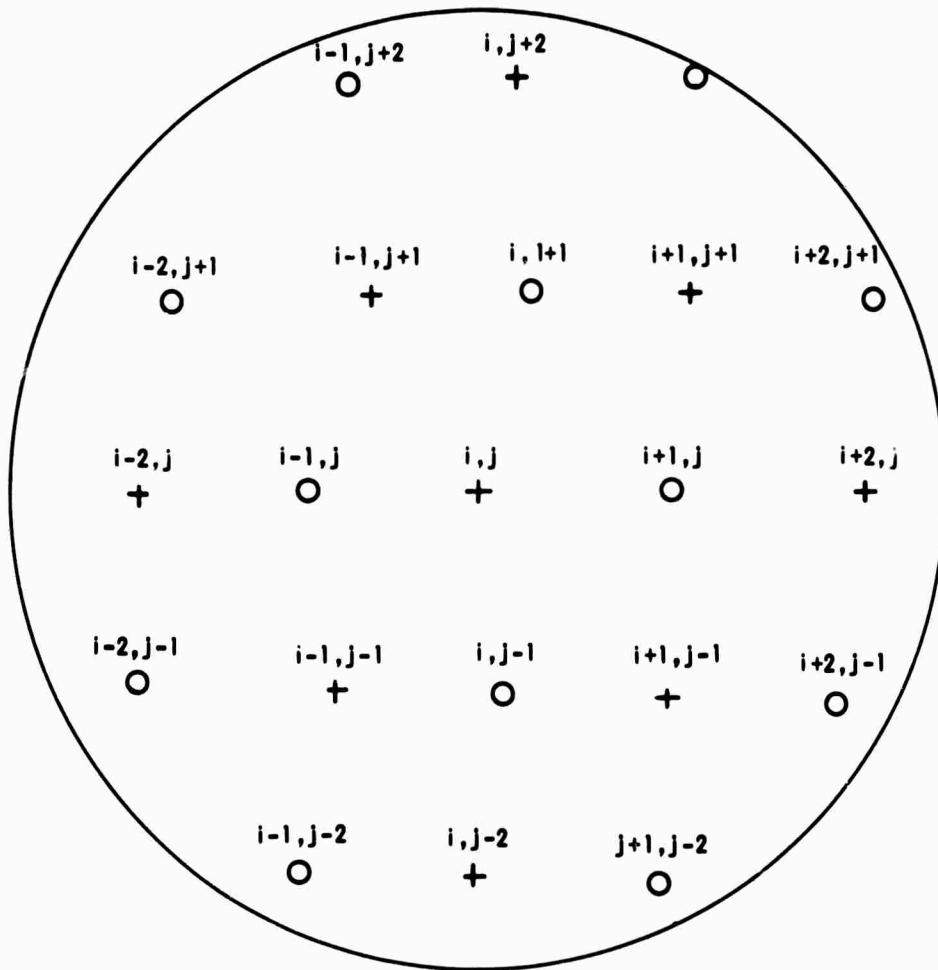


Figure 1. SOIL MOTION PATTERN AS DETERMINED FROM LEAD MARKERS  
(THREE-PERCENT SLIP)



+ MARKER POINTS  
 O VELOCITY POINTS

Figure 2. CUTOUT SHOWING CHECKERBOARD PATTERN OF MARKER AND VELOCITY POINTS

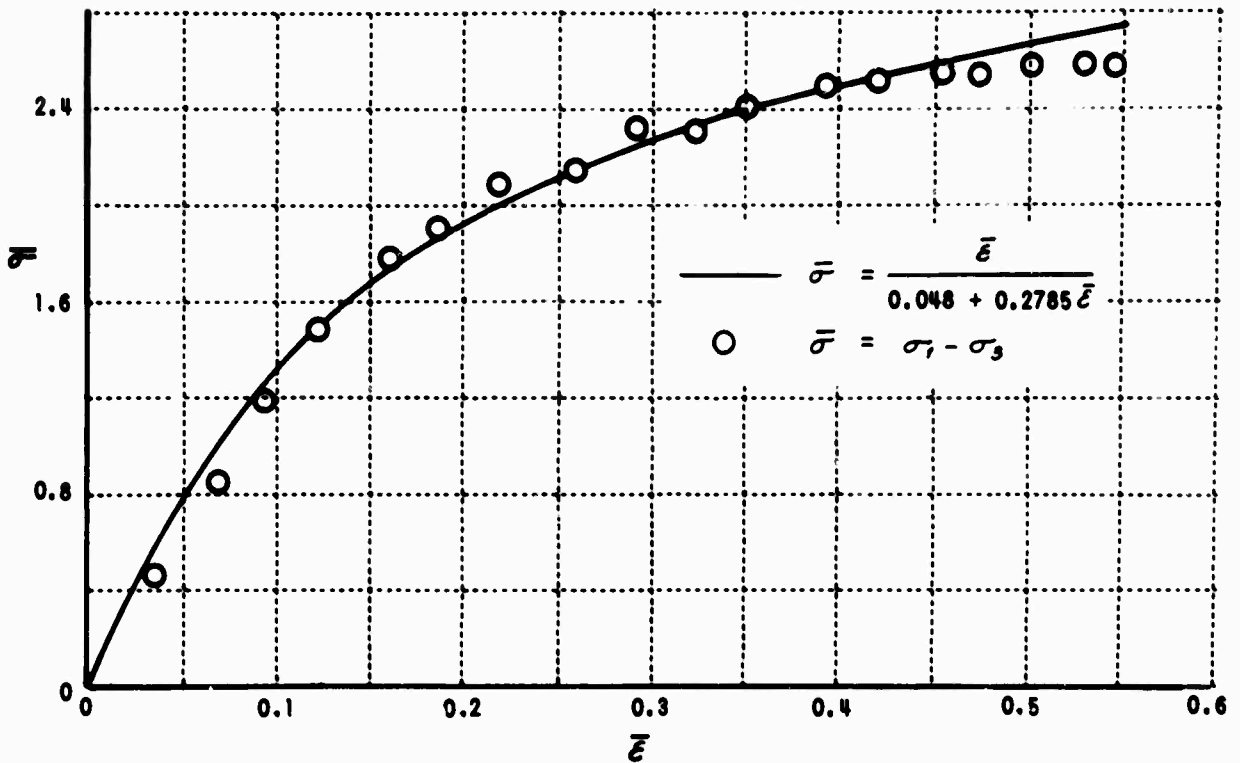


Figure 3. EQUIVALENT STRESS VS. EQUIVALENT STRAIN RELATION DETERMINED FROM TRIAXIAL TEST

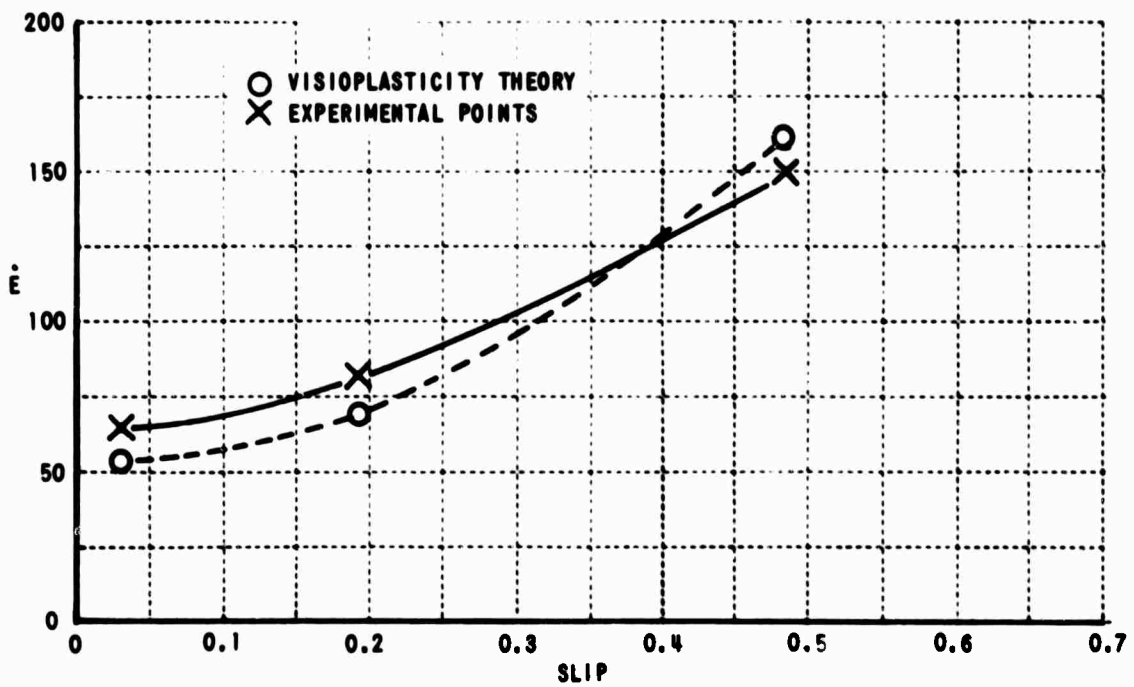


Figure 4. ENERGY DISSIPATION RATE SHOWN AS A FUNCTION OF SLIP

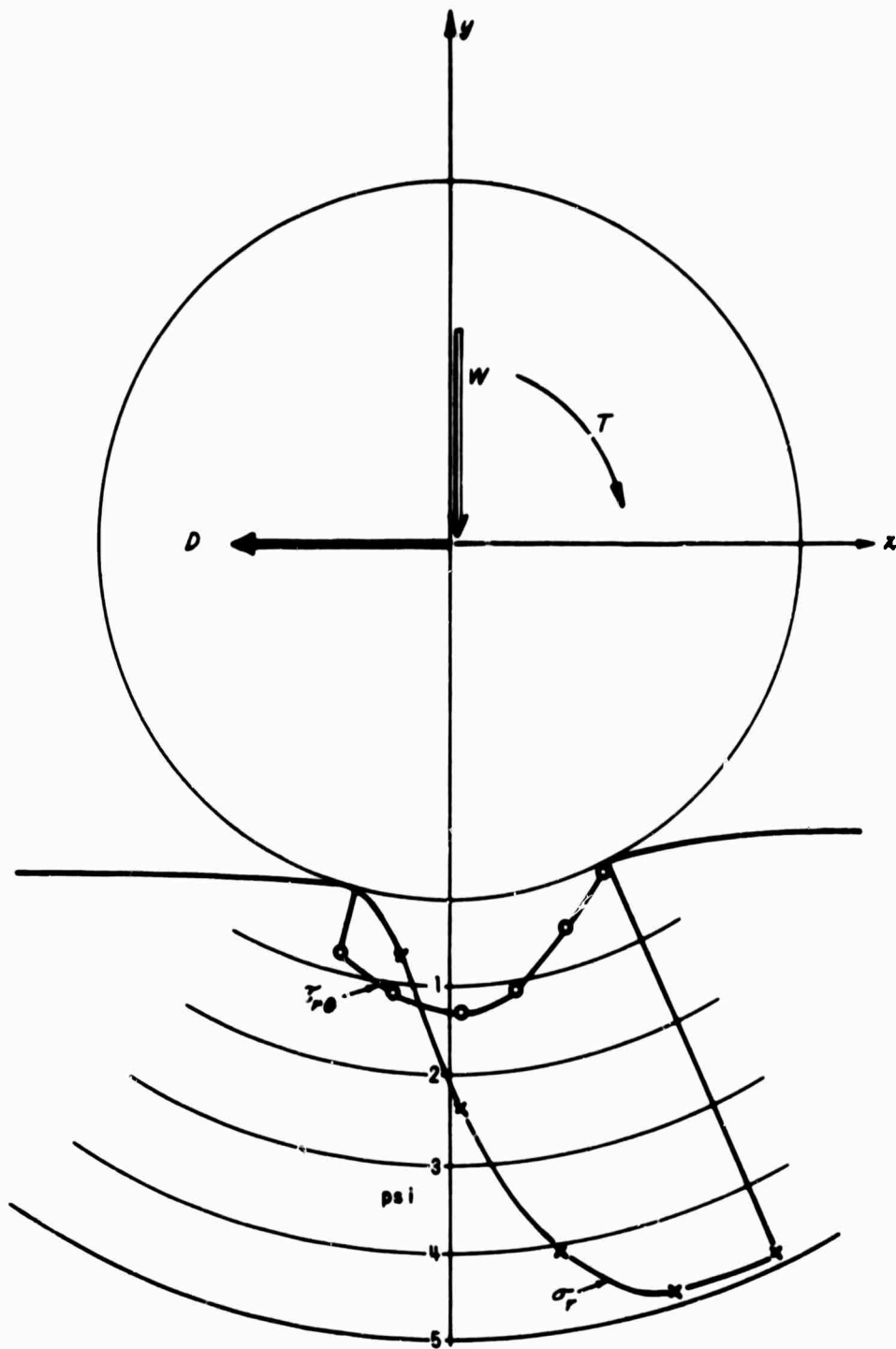


Figure 5. STRESS DISTRIBUTION CALCULATED FOR RIGID WHEEL HAVING THREE-PERCENT SLIP

**Table 1**  
**COMPARISON OF MEASURED AND CALCULATED ENERGY DISSIPATION RATES**

SLIP PERCENT	LINEAR VELOCITY in./sec	ENERGY DISSIPATION RATE in.-lb/sec			
		MEASURED	CALCULATED		
		$\dot{E}_m$	$\dot{E}_c$	$\dot{E}_s$	$\dot{E}$
3	3.1	65	49	5	54
19	3.2	80	54	15	69
48	4.1	148	75	86	161

## REFERENCES

1. Bekker, M. G. Theory of Land Locomotion University of Michigan Press Ann Arbor, Michigan 1956.
2. Bekker, M. G. Off-the-Road Locomotion University of Michigan Press Ann Arbor, Michigan 1960.
3. Bartlett, G. E., Kaufman, S., McAdams, H. T. and Smith, R. L. (coedited by) "Survey and Program Definition for Off-Road Mobility Research" First Semiannual Technical Report CAL Report VJ-2330-G-1 Cornell Aeronautical Laboratory, Inc. Buffalo, New York March 1967.
4. Thomsen, E. G., Yang, C. T. and Kobayashi, S. Mechanics of Plastic Deformation in Metal Processing MacMillan Company New York, New York 1965.
5. Yang, C. T. and Thomsen, E. G. "Plastic Flow in Lead Extrusion" Transactions of the ASME Vol 75 No. 4 May 1953 pp 575-579.
6. Thomsen, E. G. and Lapsley, Jr., J. T. "Experimental Stress Determination Within a Metal During Plastic Flow" Proceedings of the Society of Experimental Stress Analysis Vol 11 No. 2 1954 pp 59-68.
7. Shabaik, A. and Kobayashi, S. "Investigation of the Application of Visioplasticity Methods of Analysis to Metal Deformation Processing" Final Report prepared for U. S. Navy Bureau of Naval Weapons Contract NOw 65-0374-d February 1966.
8. Bartlett, G. E., Kaufman, S. and Deutschman, J. N. (edited by) "Off-Road Mobility Research" Second Semiannual Technical Report CAL Report VJ-2330-G-2 Cornell Aeronautical Laboratory, Inc. Buffalo, New York September 1967.
9. Yong, R. N. and Osler, J. C. "On the Analysis of Soil Deformation Under a Moving Rigid Wheel" Proceedings of the Second International Conference of ISTVS Quebec, Canada 1966 pp 339-352.
10. Boyd, C. W. and Windisch, S. J. "A Technique for Measuring Deformations Within a Sand Under Controlled Wheel Loads" Proceedings of the Second International Conference of ISTVS Quebec, Canada 1966 pp 183-197.
11. Yong, R. N., Boyd, C. W. and Webb, G. L. "Experimental Study of Behavior of Sand Under Moving Rigid Wheels" Soil Mechanics Series Report 20 McGill University Montreal, Canada August 1967.

12. Arthur, J. R. F., James, R. G. and Roscoe, K. H. "Determination of Stress Fields During Plane Strain of a Sand" *Geotechnique* Vol 14 No. 4 1965 pp 283-308.
13. Burland, J. B. "Deformation of Soft Clay" PhD Dissertation Cambridge University Cambridge, England 1967.
14. Henkel, D. J., Esrig, M. I., Steinbach, J. and Yudhbir "Some Aspects of Soil Mechanics in Relation to Vehicle Mobility" *Soil Engineering Series Research Report 5* Cornell University Ithaca, New York February 1968.
15. Henkel, D. J., Esrig, M. I., Steinbach, J. and Yudhbir "Report on the Use of Consolidated and Artificial Soils for the Laboratory Study of Vehicle Mobility" *Soil Engineering Series Research Report 8* Cornell University Ithaca, New York July 1968.
16. Prager, W. Introduction to Mechanics of Continua Ginn and Co. New York, New York 1961.
17. Hill, R. The Mathematical Theory of Plasticity University Press Oxford, England 1950.
18. Osgood, W. R. "Stress-Strain Formulas" *Journal of Aeronautical Science* Vol 13 1949 pp 45-48.
19. Kondner, R. L. "Hyperbolic Stress-Strain Response; Cohesive Soils" *Journal of the Soil Mechanics and Foundation Division ASCE* Vol 89 1963 pp 115-143.
20. Perzyna, P. "The Constitutive Equations for Rate-Sensitive Plastic Material" Advances in Applied Mechanics Academic Press New York, New York Vol 9 1966.
21. Paslay, P. R. and Slibar, A. "Laminar Flow of Drilling-Mud Due to Axial Pressure Gradient and External Torque" *Petroleum Transactions of AIME* Vol 210 1957 pp 310-317.
22. Drucker, D. C. Greenberg, H. J. and Prager, W. "The Safety Factor of an Elastic-Plastic Body in Plane Strain" *Transactions of ASME Series E Journal of Applied Mechanics* Vol 18 1951 pp 371-378.
23. Onafeko, O. and Reece, A. R. "Soil Stresses and Deformations Beneath Rigid Wheels" *Journal of Terra Mechanics* Vol 4 No. 1 1967 pp 59-80.
24. Yong, R. N. Private Communication.

APPENDIX I  
COORDINATE TRANSFORMATIONS AND  
DATA-SMOOTHING TECHNIQUES

I-1. Coordinate Transformations

There are actually two transformations required in order to place the data in the assumed steady-state coordinate system; i. e., from the film plane to the marker plane and from the fixed marker coordinate system to the moving system.

A schematic representation of the experimental setup is shown in Figure I-1. Since all measurements are made on X-ray film, they represent a magnification of the actual distances in the physical plane of the markers. If we let  $(x_f, y_f)$  represent points in the film plane and  $(x_m, y_m)$  corresponding points in the marker plane, then it is readily seen that the required transformation is

$$\begin{aligned}x_m &= \mu x_f \\y_m &= \mu y_f\end{aligned}\tag{I-1}$$

where

$$\mu = \frac{z_{s0}}{z_{f0}}$$

with  $z_{s0}$  and  $z_{f0}$  the distances, respectively, from the X-ray optical center to the marker plane and film plane.

This transformation is followed by a single translation from the fixed coordinate system of the marker plane to that moving with the wheel denoted by  $(x, y)$ . As is shown in Figure I-1, the coordinate distances from the wheel axle to the optical center are given by  $[D_1(t_i), D_2(t_i)]$ . Since three X-ray shots were taken during the test,  $D_1(t_i)$  takes on three values whose successive difference is 6 inches, while  $D_2(t_i)$  remains constant. At any given time, the following transformation applies:

$$\begin{aligned}x &= x_m + D_1(t_i) \\y &= y_m - D_2(t_i)\end{aligned}\tag{I-2}$$

## 1-2. Data Smoothing of Flow Pattern

It is assumed that there are two kinds of inaccuracies in the data. The analysis requires that all points initially lie on a straight, horizontal line and the first X-ray shot indicates a slight departure. Furthermore, inaccuracies result from the basic problems of measurement and control, particularly in the matching of the results from one shot to the next.

From the measurements of the first X-ray film (undisturbed markers), the  $y$  coordinate values are averaged. Then, for each marker, the deviation from this mean is determined. This deviation is then added to the  $y$  coordinate value of the same marker in successive X-ray film. It is believed that this adjustment represents a first-order correction which tends to account for small departures from a purely horizontal alignment in the initial configuration.

Since the relative times,  $t_i$ , are known for all markers in the X-ray photographs taken during the test, the coordinate values of each marker are expressed as  $[x(t_i), y(t_i)]$ . Thus, the measured values at each marker are expressed as a function of the time  $t$ . For a marker point in any row, a second-order polynomial is fitted to the  $x$  values and also the  $y$  values using  $t$  as the independent variable. Five points, centered about the marker point, are employed with additional constraints in the least squares sense. The corrected value is obtained by evaluating the curve fit function at the known value of  $t_i$ . This scheme is applied to all data points on the three X-ray photographs taken during the test.

## 1-3. Velocity Interpolation Scheme

Since the velocity components are not available on a regular grid, some interpolation is required. Furthermore, it was found that some data smoothing was required because of the matching problem and also to permit more flexibility in the interpolation subroutine. A general surface-fitting subroutine was developed.

For example, if we wish to fit a function  $P(x,y)$  about the point  $(x^*, y^*)$ , let

$$P(x,y) = a_0 + a_1(x-x^*) + a_2(y-y^*) + a_3(x-x^*)^2 + a_4(y-y^*) + a_5(x-x^*)(y-y^*). \quad (1-3)$$

Thus, at least six data points are required and, if more are given, the normal equations may be developed using traditional least squares constraints. The subroutine is organized so that any number of points may be specified. In the surface fitting for the velocity components, where derivatives are desired at the marker point  $(i,j)$ , the twelve nearest neighboring velocity points were specified. This selection of points is modified slightly on the boundary and adjacent rows where one-sided derivatives must be calculated.

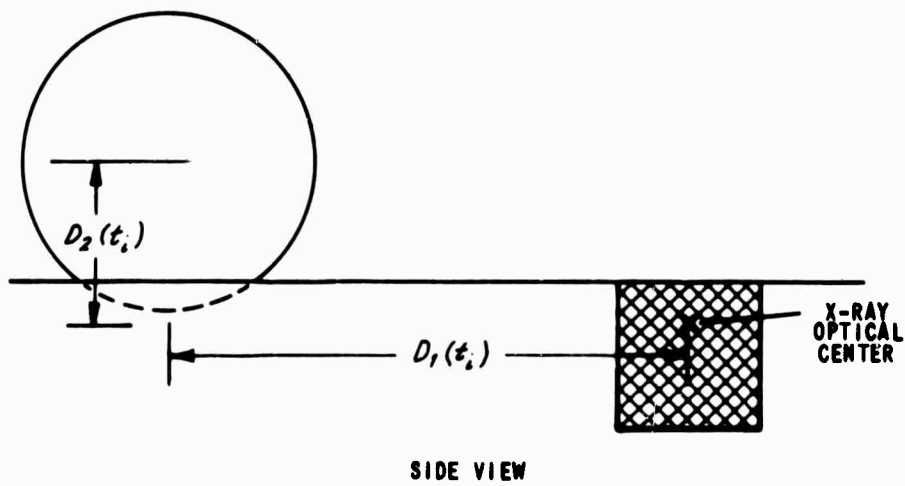
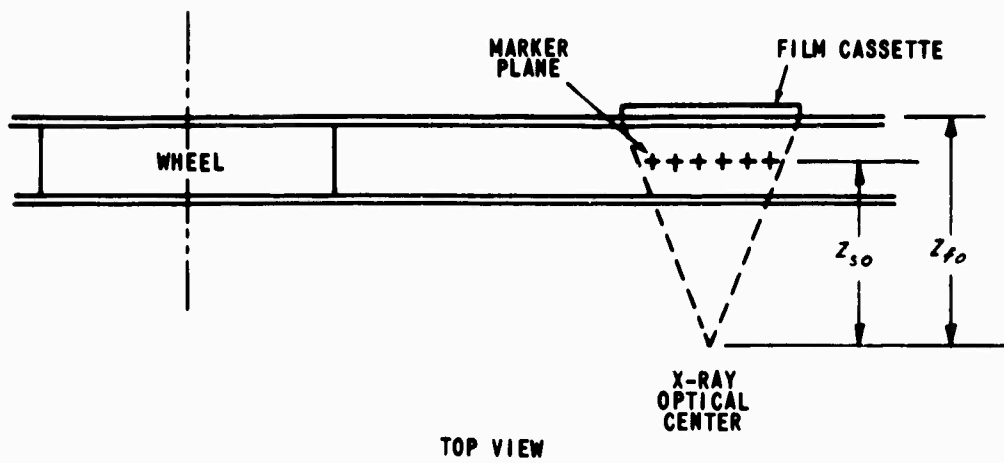


Figure I-1. SCHEMATIC REPRESENTATION SHOWING EXPERIMENTAL FACILITY

## APPENDIX II

### TENSOR NOTATION AND DEFINITIONS

A more complete description of the properties of the stress, strain and strain-rate tensors can be found in most continuum mechanics textbooks. In the following, however, we present a very brief review of some of the more important properties and definitions for the stress and strain tensors.

Stress and strain are second-order tensors and, for example, the stress tensor,  $\sigma_{ij}$ , has nine components since  $i$  and  $j$  each take on values one through three. These indices correspond to spacial coordinates such as  $x$ ,  $y$  and  $z$ . With the indicial notation, repeated indices indicate summation; e. g.,

$$\sigma_{kk} = \sigma_{11} + \sigma_{22} + \sigma_{33} = \sigma_x + \sigma_y + \sigma_z. \quad (\text{II-1})$$

The Kronecker delta,  $\delta_{ij}$ , is defined as zero when  $i$  and  $j$  differ and unity when  $i$  and  $j$  have the same value. Thus,

$$\delta_{i,j} = \begin{cases} 0 & \text{if } i \neq j \\ 1 & \text{if } i = j. \end{cases} \quad (\text{II-2})$$

The following definitions are made for the stress tensor,  $\sigma_{ij}$ , and the strain tensor,  $\epsilon_{ij}$ :

- (a) hydrostatic or mean stress,  $p$ ,

$$p = -\frac{1}{3} \sigma_{kk} \quad (\text{II-3})$$

- (b) stress deviator tensor,  $S'_{ij}$ ,

$$S'_{ij} = \sigma_{ij} + p\delta_{ij} \quad (\text{II-4})$$

- (c) mean strain,  $e$ ,

$$e = \frac{1}{3} \epsilon_{kk} \quad (\text{II-5})$$

(d) strain deviator tensor,  $e_{ij}$ ,

$$e_{ij} = \epsilon_{ij} - e\delta_{ij}. \quad (\text{II-6})$$

The invariants of a tensor are determined from its characteristic equation. For example, with the stress tensor,  $\sigma_{ij}$ , the characteristic equation is the determinant equated to zero,

$$|\sigma_{ij} - \sigma\delta_{ij}| = 0 \quad (\text{II-7})$$

which is equivalent to the cubic equation

$$\sigma^3 + I_1\sigma^2 + I_2\sigma + I_3 = 0. \quad (\text{II-8})$$

The coefficients  $I_1$ ,  $I_2$  and  $I_3$  are, respectively, the first, second and third invariants of the stress tensor. The principal stresses,  $\sigma_1$ ,  $\sigma_2$ , and  $\sigma_3$  are the roots of the cubic equation.

APPENDIX III  
CYLINDRICAL SOIL MECHANICS TEST

In the cylindrical or so-called triaxial soil mechanics test, cylindrical soil specimens are subjected to controlled longitudinal deformations and lateral pressures. For the undrained test on saturated clay soils, the behavior is almost incompressible. In order to satisfy the requirements of the viscoplasticity, it is necessary to interpret the results in terms of equivalent stress and equivalent strain parameters.

A cylindrical coordinate system  $(r, \theta, z)$  is selected such that the  $z$  coordinate corresponds to the longitudinal axis of the cylinder. Throughout the test, it is assumed that  $\sigma_r, \sigma_\theta, \sigma_z$  and  $\epsilon_r, \epsilon_\theta, \epsilon_z$  are the only nonzero stresses and strains, respectively. It is also postulated that

$$\begin{aligned}\sigma_r &= \sigma_\theta \\ \epsilon_r &= \epsilon_\theta.\end{aligned}\tag{III-1}$$

For the incompressible medium,

$$\epsilon_r = -\frac{1}{2}\epsilon_z.\tag{III-2}$$

The mean stress,  $p$ , is

$$p = -\frac{1}{3}(\sigma_z + 2\sigma_r).\tag{III-3}$$

As a result, the stress deviator components are

$$\begin{aligned}s_z &= \frac{2}{3}(\sigma_z - \sigma_r) \\ s_r = s_\theta &= -\frac{1}{3}(\sigma_z - \sigma_r).\end{aligned}\tag{III-4}$$

For this test, the Levy-Mises equation [see Equation (3.7)]

$$\dot{\epsilon}_{ij} = \frac{3}{2} \frac{\dot{\epsilon}}{\sigma} s_{ij}\tag{III-5}$$

becomes

$$\dot{\epsilon}_y = \frac{3}{2} \frac{\dot{\bar{\epsilon}}}{\bar{\sigma}} \sigma_y = \frac{\dot{\bar{\epsilon}}}{\bar{\sigma}} (\sigma_y - \sigma_r). \quad (\text{III-6})$$

By definition, the equivalent stress is

$$\bar{\sigma} = \left\{ \frac{1}{2} \left[ (\sigma_r - \sigma_\theta)^2 + (\sigma_\theta - \sigma_y)^2 + (\sigma_y - \sigma_r)^2 \right] \right\}^{\frac{1}{2}} \quad (\text{III-7})$$

or, substituting Equations (III-1) in Equation (III-7),

$$\bar{\sigma} = (\sigma_y - \sigma_r). \quad (\text{III-8})$$

As a consequence,

$$\frac{\dot{\epsilon}_y}{\dot{\bar{\epsilon}}} = \frac{d\epsilon_y}{d\bar{\epsilon}} = \frac{\epsilon_y}{\bar{\epsilon}} = 1. \quad (\text{III-9})$$

Thus, during the test, there is a one-to-one correspondence between the strain increment and the finite strain, and the curve  $(\sigma_y - \sigma_r)$  versus  $\epsilon_y$  can be taken as the required relation between  $\bar{\sigma}$  and  $\bar{\epsilon}$ .

## APPENDIX IV

### CALCULATION OF STRESSES IN THE SOIL - WHEEL INTERFACE

Consider the polar coordinate system attached to the rigid wheel as shown in Figure IV-1. In the system strain rates,  $\dot{\epsilon}_r$ ,  $\dot{\epsilon}_\theta$ , and  $\dot{\gamma}_{r\theta}$ , and the equivalent strain rate,  $\dot{\bar{\epsilon}}$ , are determined from the measured velocity field. The equivalent stress,  $\bar{\sigma}$ , is determined from the stress-strain curve. A solution, in the viscoplastic sense, means that the stresses,  $\sigma_r$ ,  $\sigma_\theta$  and  $\tau_{r\theta}$ , must be determined as functions of these measured variables.

The plasticity relations for an incompressible, Levy-Mises theory are

$$\begin{aligned}\dot{\epsilon}_r &= \frac{3}{2} \frac{\dot{\bar{\epsilon}}}{\bar{\sigma}} (\sigma_r + p) \\ \dot{\epsilon}_\theta &= \frac{3}{2} \frac{\dot{\bar{\epsilon}}}{\bar{\sigma}} (\sigma_\theta + p) \\ \dot{\gamma}_{r\theta} &= 3 \frac{\dot{\bar{\epsilon}}}{\bar{\sigma}} \tau_{r\theta}\end{aligned}\tag{IV-1}$$

where

$$p = -\frac{1}{3} (\sigma_r + \sigma_\theta + \sigma_z),^*$$

The hydrostatic pressure,  $p$ , may be eliminated, yielding

$$\begin{aligned}\sigma_r - \sigma_\theta &= \frac{2}{3} \frac{\bar{\sigma}}{\bar{\epsilon}} (\dot{\epsilon}_r - \dot{\epsilon}_\theta) \\ \tau_{r\theta} &= \frac{1}{3} \frac{\bar{\sigma}}{\bar{\epsilon}} \dot{\gamma}_{r\theta}.\end{aligned}\tag{IV-2}$$

---

\*The engineering shear strain rate,  $\dot{\gamma}_{r\theta}$ , is used here; i. e.,  $\dot{\gamma}_{r\theta} = 2\dot{\epsilon}_{r\theta}$ .

The equilibrium equations in polar coordinates are

$$\begin{aligned} \frac{\partial \sigma_r}{\partial r} + \frac{1}{r} \frac{\partial \tau_{r\theta}}{\partial \theta} + \frac{\sigma_r - \sigma_\theta}{r} &= 0 \\ \frac{\partial \tau_{r\theta}}{\partial r} + \frac{1}{r} \frac{\partial \sigma_\theta}{\partial \theta} + \frac{2 \tau_{r\theta}}{r} &= 0. \end{aligned} \quad (\text{IV-3})$$

Substitution of Equations (IV-2) into the first equilibrium equation gives

$$\frac{\partial \sigma_r}{\partial r} = -\frac{2}{3} \frac{1}{r} \left[ \frac{\bar{\sigma}}{\bar{E}} (\dot{\epsilon}_r - \dot{\epsilon}_\theta) + \frac{1}{2} \frac{\partial}{\partial \theta} \left( \frac{\bar{\sigma}}{\bar{E}} \dot{\gamma}_{r\theta} \right) \right]. \quad (\text{IV-4})$$

Integrate to obtain

$$\sigma_r = -\frac{2}{3} \int_R^r \frac{1}{r'} \left[ \frac{\bar{\sigma}}{\bar{E}} (\dot{\epsilon}_r - \dot{\epsilon}_\theta) + \frac{1}{2} \frac{\partial}{\partial \theta} \left( \frac{\bar{\sigma}}{\bar{E}} \dot{\gamma}_{r\theta} \right) \right] dr' + K(\theta) \quad (\text{IV-5})$$

where  $R$  is the wheel radius and the integration function,  $K(\theta)$ , is the value of  $\sigma_r$  at  $r = R$ . Since the stresses are required at the interface, the problem is reduced to determining  $K(\theta)$ .

To determine  $K(\theta)$ , differentiate the first of Equations (IV-2) with respect to  $\theta$ , use Equation (IV-2) to eliminate  $\sigma_r$ , then substitute this equation along with the second plasticity equation into the second equilibrium, Equations (IV-3). This results in

$$\begin{aligned} -\frac{2}{3} \int_R^r \frac{\partial}{\partial \theta} \left\{ \frac{1}{r'} \left[ \frac{\bar{\sigma}}{\bar{E}} (\dot{\epsilon}_r - \dot{\epsilon}_\theta) + \frac{1}{2} \frac{\partial}{\partial \theta} \left( \frac{\bar{\sigma}}{\bar{E}} \dot{\gamma}_{r\theta} \right) \right] \right\} dr' + \frac{\partial K(\theta)}{\partial \theta} \\ -\frac{2}{3} \frac{\partial}{\partial \theta} \left[ \frac{\bar{\sigma}}{\bar{E}} (\dot{\epsilon}_r - \dot{\epsilon}_\theta) \right] + \frac{2}{3} r \left[ \frac{1}{2} \frac{\partial}{\partial r} \left( \frac{\bar{\sigma}}{\bar{E}} \dot{\gamma}_{r\theta} \right) + \frac{1}{r} \frac{\bar{\sigma}}{\bar{E}} \dot{\gamma}_{r\theta} \right] = 0. \end{aligned} \quad (\text{IV-6})$$

If  $r = R$ , then the integral in the above equation is zero. Solving for  $K(\theta)$ , yields

$$\frac{\partial K(\theta)}{\partial \theta} = \frac{2}{3} \left\{ \frac{\partial}{\partial \theta} \left[ \frac{\bar{\sigma}}{\bar{E}} (\dot{\epsilon}_r - \dot{\epsilon}_\theta) \right] - r \left[ \frac{1}{2} \frac{\partial}{\partial r} \left( \frac{\bar{\sigma}}{\bar{E}} \dot{\gamma}_{r\theta} \right) + \frac{1}{r} \frac{\bar{\sigma}}{\bar{E}} \dot{\gamma}_{r\theta} \right] \right\}_{r=R}. \quad (\text{IV-7})$$

The function,  $K(\theta)$ , is obtained through integration with respect to  $\theta$  and observing that  $\sigma_r = 0$  at  $r = R$  and  $\theta = \theta_0$ ; i. e.,

$$K(\theta) = \frac{2}{3} \left\{ \left[ \frac{\bar{\sigma}}{\bar{E}} (\dot{E}_r - \dot{E}_\theta) \right]_{\theta_0}^{\theta} - R \int_{\theta_0}^{\theta} \left[ \frac{1}{2} \frac{\partial}{\partial r} \left( \frac{\bar{\sigma}}{\bar{E}} \dot{\gamma}_{r\theta} \right) + \frac{1}{R} \frac{\bar{\sigma}}{\bar{E}} \dot{\gamma}_{r\theta} \right] d\theta \right\}_{r=R}. \quad (\text{IV-8})$$

As a result of Equations (IV-5) and (IV-2), the stress in the soil - wheel interface are given by

$$\sigma_r \Big|_{r=R} = K(\theta)$$

$$\sigma_\theta \Big|_{r=R} = K(\theta) - \left[ \frac{2}{3} \frac{\bar{\sigma}}{\bar{E}} (\dot{E}_r - \dot{E}_\theta) \right]_{r=R}$$

$$\tau_{r\theta} \Big|_{r=R} = \left[ \frac{1}{3} \frac{\bar{\sigma}}{\bar{E}} \dot{\gamma}_{r\theta} \right]_{r=R}.$$

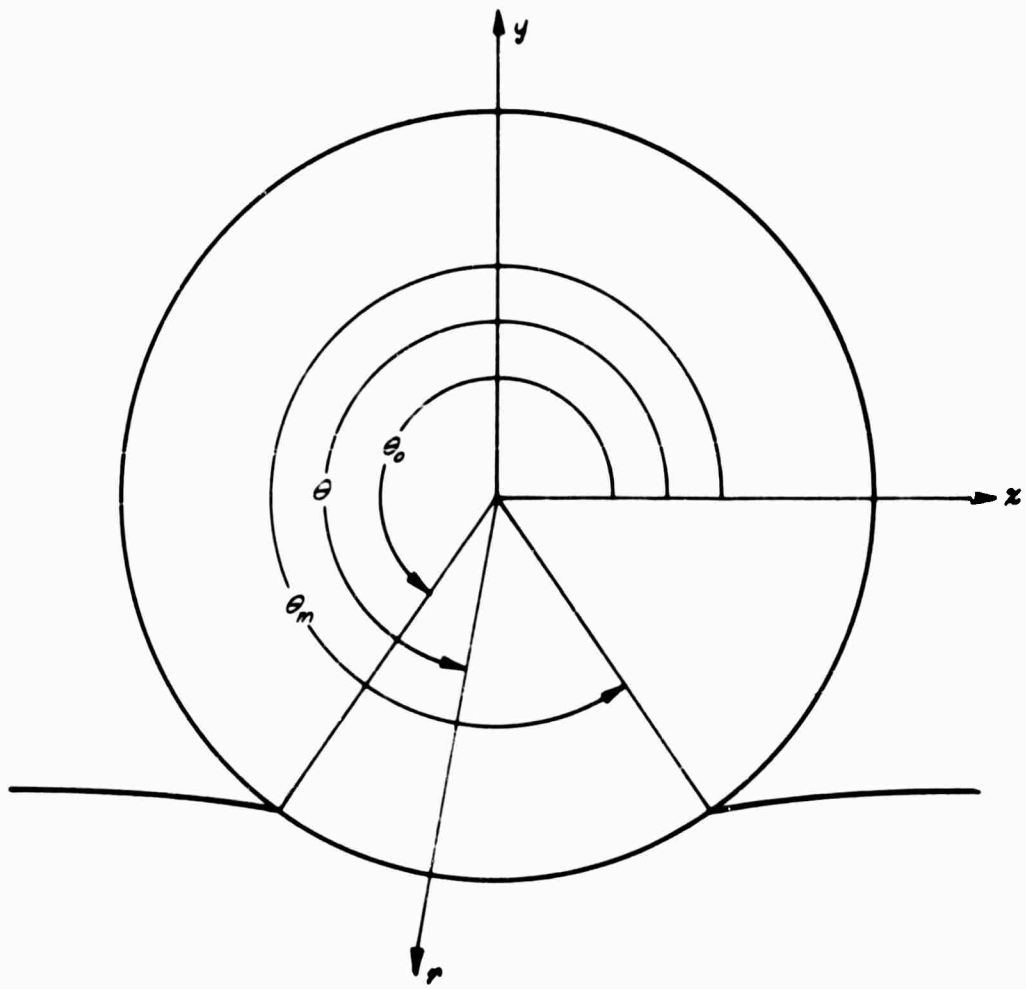


Figure IV-1. COORDINATE SYSTEM USED FOR STRESS ANALYSIS